Chapter 4

Size dependent properties of SnO_2 and TiO_2 nanostructures

4.1 Thermodynamic properties in SnO_2 nanoparticles

Nano structured oxides have attracted considerable attention in recent times due to their novel properties and application prospects in electronics and devices. Various interesting properties can be obtained when size of the material is reduced to nanometer scale compared to its bulk counterpart [4.1]. Titanium and tin dioxide are important oxides in opto-electronic technologies involving efficient dielectrics, catalysis, sensors, thin film transistors, nano biotechnology and other transparent electronic devices [4.2-4.12].

4.1.1 Melting temperature

The melting of nanocrystals has received considerable attention since 1954 when Takagi experimentally demonstrated that the ultrafine metallic nanocrystals melt below their corresponding bulk melting temperature $T_m(\infty)$ with ∞ denoting the bulk [4.13]. In the present section, we present the results based on our calculations on the effects of size and shape on melting temperature of tin dioxide (SnO_2) nanoparticles. To calculate size and dimension dependent melting temperature of SnO_2 nanoparticles we have used the following equation which is derived in chapter 2.

$$\frac{T_m(r)}{T_m(\infty)} = \frac{\sigma^2(\infty)}{\sigma^2(r)} = exp\left\{\frac{-(\alpha-1)}{[(r/r_0)-1]}\right\} \qquad ...(1)$$

where, $\alpha=2S_{vib}(\infty)/(3R)+1$ and $r_0=(3-d)h$.

Effect of dimension has been evaluated by taking different values of dimension *(d)* in the eqn.(1) which corresponds to the spherical nanoparticles, nano wire (tubes) and thin film like materials. Our calculated data are presented in Table 4.1.

[Table 4.1]

Calculated results of size dependent melting temperature of SnO_2 nanoparticles

Size of SnO_2 nanoparticles (nm)	**Melting temperature, T_m (K) Different shapes of SnO_2 nano particles**		
	0-d (spherical particle)	1-d (nano wire)	2-d (thin film)
1	1120.66	1512.58	1747.79
2	1643.5	1747.79	1832.65
3	1747.79	1806.19	1857.5
4	1792.3	1832.65	1869.4
5	1816.96	1847.76	1876.36
6	1832.65	1857.5	1880.93
7	1843.49	1864.36	1884.14
8	1851.45	1869.4	1886.55
9	1857.5	1873.27	1888.41
10	1862.3	1876.36	1889.89
11	1866.19	1878.84	1891.09

12	1869.4	1880.93	1892.1
13	1872.09	1882.66	1892.95
14	1874.37	1884.14	1893.68
15	1876.36	1885.45	1894.31
16	1878.07	1886.55	1894.86
17	1879.57	1886.63	1895.34
18	1880.93	1888.41	1896.76
19	1882.11	1889.19	1896.14
20	1883.01	1889.86	1896.49
40	1893.2	1896.33	1899.00
60	1896.33	1896.62	1900.84

From the above data, it is found that the melting temperature of SnO_2 nanoparticles decreases as the size of the particle decreases, similar to previous observations on metal nanoparticles [4.14-4.16]. The calculated melting temperature of SnO_2 nanoparticles as a function of size and dimension is presented in Fig. 4.1. Melting is a surface phenomena therefore it is obvious that it is affected by surface area of material. Nanoparticles have large surface area as compared to bulk materials thereby they melt at lower temperature. Figure depicts with increase in particle size, melting temperature also increases and after 50 nm it becomes

almost constant with size. At this point, nanoparticles will have value of melting temperature (T_m) nearly equal to bulk melting temperature that is around 1850K. Below 20nm, there is considerable difference in T_m for the different dimensions of SnO_2 nanoparticles. Spherical nanoparticles (0-d) show lower value of T_m compared to 1-d and 2-d particles.

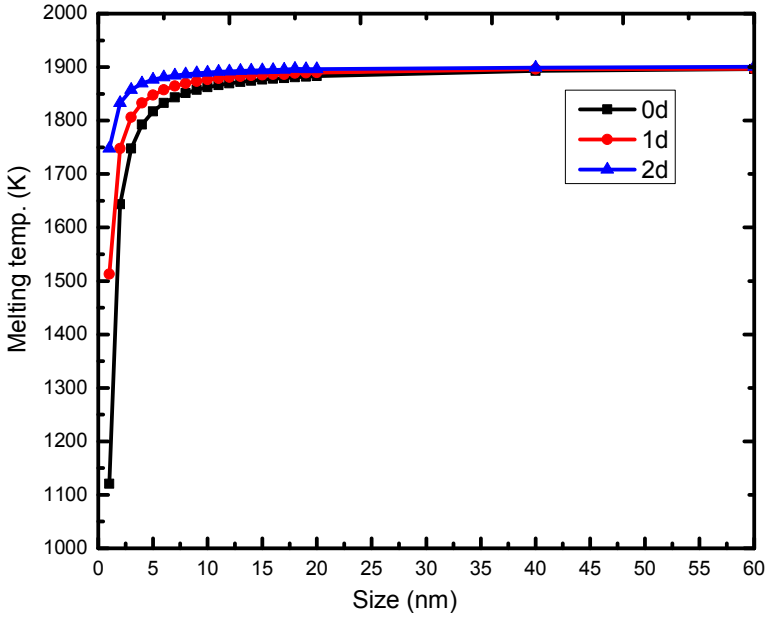

[Fig. 4.1]

The related parameters to calculate size dependent melting temperature of SnO_2 nanoparticles are h=0.2057nm $T_m(\infty)$=1903K and $S_{vib}(\infty)$=4.098 $Jmol^{-1}K^{-1}$ [4.17].

4.1.2 Glass-transition temperature

Glasses are characterized by their short range order of atomic arrangement. They are hard and brittle object while rubbery materials have flexible and elastic characteristics. A typical glass transition is the temperature at which material changes from hard and brittle state to rubbery state. Fig. 4.2 presents the variation of glass transition T_g with the size for SnO_2 nanoparticles.

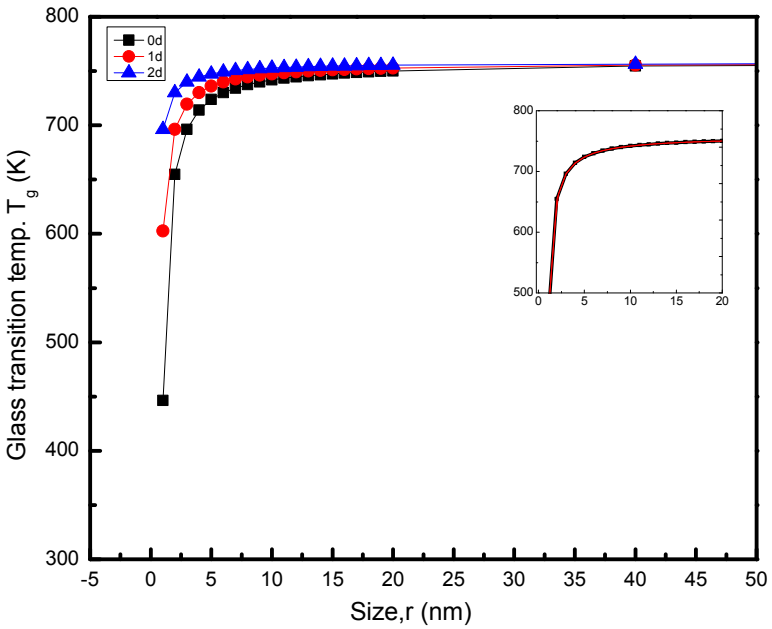

[Fig. 4.2]

This figure reveals that the glass transition temperature of SnO_2 nanoparticles increases with increase in the size of the SnO_2 nanoparticles and finally approaches to bulk glass transition temperature value, of 758K at around 40 nm. The value of glass transition temperature of bulk SnO_2 is taken from ref. [4.18]. We have found similarity between size variations of glass transition and melting temperatures of SnO_2 nanoparticles. There is a rapid drop of the glass transition temperature below 10 nm which is similar to the variation of melting temperature. This is due to the fact that as the size of nanoparticles decreases, surface area to volume ratio increases. Because of that, there will be more number of surface atoms which are more reactive and loosely bound. These atoms are responsible for the decrease in glass transition of SnO_2 nanoparticles. Rapid drop of Tg at 10 nm may be due to the Lindemann's criterion which demonstrates that the root mean square value of amplitude thermal vibration of atoms

in SnO_2 nanoparticles reaches critical value at 10 nm, a sharp drop is observed. The molecular dynamics simulation of Hoang [4.19] observed that the glass transition temperature increases with the decrease in the size of the TiO_2 nanoparticles which contradicts our results as well as the general nature of glass transition temperature [4.1].

4.1.3 Kauzmann temperature

The value of Kauzmann temperature can be used to calculate Gibbs free energy of crystallization and consequently glass forming ability of any material can be obtained [4.1].

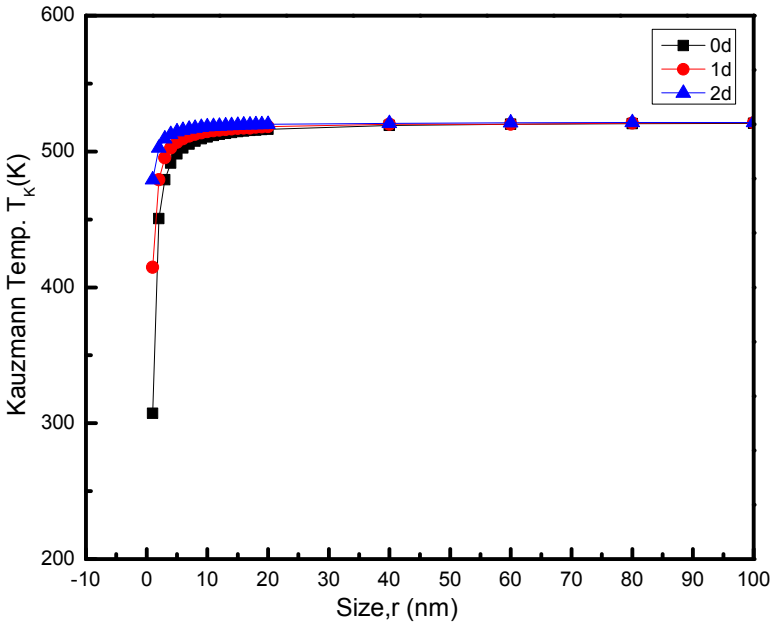

[Fig. 4.3]

Fig. 4.3 presents the size dependent Kauzmann temperature of SnO_2 nanoparticles. This figure shows that the Kauzmann temperature of SnO_2 nanoparticles depends on size of the nanoparticles similar to the melting and glass transition temperatures. However, the value of Kauzmann temperature, T_K lies below the glass transition T_g.

4.2 Diffusion co-efficient in SnO_2 nanoparticles

When size approaches to nanometer scale several of the material properties such as structural and magnetic properties, glass-to-crystal transition, and surface morphology drastically change from its bulk counterpart. These properties are strongly influenced by self-diffusion of the constituents. In addition to this, self diffusion mechanism plays an important role in the control of the long-standing application of devices based on amorphous and nano crystalline alloys [4.20]. We have carried out the calculations on size and dimension dependent diffusion coefficient of SnO_2 nanoparticles in the case of self diffusion. Diffusion coefficient of nitrogen diffused SnO_2 have also been calculated as the function of size and dimension.

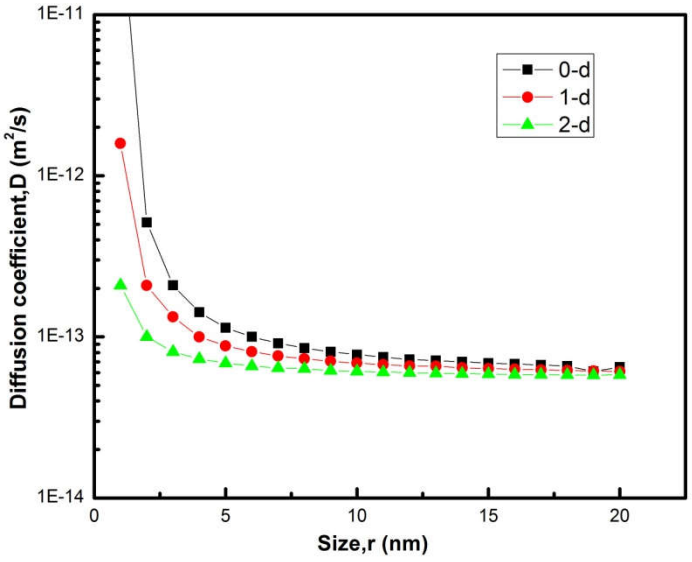

[Fig. 4.4]

Fig.4.4 shows the variation of diffusion coefficient D(r.T) with size and dimensions of SnO_2 nanoparticles. The parameters used to calculate diffusion coefficients are h = 0.2057 nm , T = 573 K, $S_{vib}(\infty) = 4.098 Jmol^{-1}K^{-1}$, $D_0 = 0.02\times10^{-2}\ m^2s^{-1}$ and $E(\infty) = 86.731 KJmol^{-1}$[4.17,4.21].

It can be observed that the diffusion coefficient for zero dimensional SnO_2 nanoparticles (spherical) is higher than one and two dimensional SnO_2 nanostructures (i.e., cylindrical wire and thin film). It implies faster diffusion mechanism in the case of spherical nanoparticles. It is clear from the figure that the diffusion coefficient increases as size of the SnO_2 particles decreases. However, there is a considerable difference for the smaller size but values of diffusion coefficients are constant with size and nearly equal for all the three dimensions when particle size exceeds 10 nm.

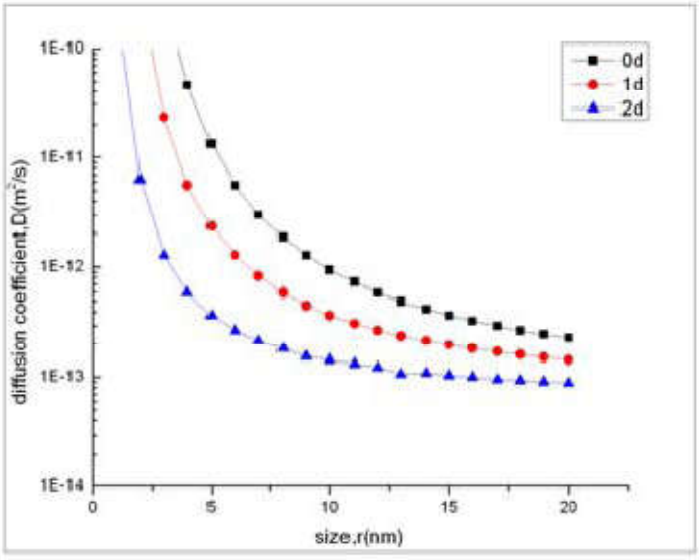

[Fig.4.5]

Fig.4.5 presents diffusion coefficients of nitrogen diffused SnO_2 for different dimensions and sizes. The value of activation energy for bulk system is 78.3 $KJmol^{-1}$ [4.22]. For nitrogen doping activation energy decreases with size and consequently diffusion coefficient increases. Nitrogen doping has received considerable attention compared to the other anionic elements because of its comparable atomic size with oxygen, small ionization

energy, meta stable centre formation and stability [4.23-4.26]. In conclusion, we have investigated that diffusion coefficients of SnO_2 nanoparticles in the case of self diffusion and diffused with nitrogen. Nanoparticles are strongly influenced by the size and dimensions. Diffusion coefficient increases as the size of the SnO_2 nanoparticles decreases. In addition to that higher value of diffusion coefficient in the case spherical SnO_2 nanoparticles indicates faster diffusion mechanism for zero dimension than one and two dimensional nanostructures [4.27].

4.3 Surface properties in SnO_2 and TiO_2 nanoparticles

As large surface to volume ratio possesses the key importance for nanomaterials, surface energy (tension) thereby can be considered as a fundamental physical quantity to understand the surface effects like crystal growth, nucleation, surface faceting, growth and stability of thin films, etc [4.28-4.30]. In addition, the surface tension plays an important role in a variety of scientific and industrial applications. The surface tension influences distillation, condensation, gas absorption and emission and excitation a part from being an important basic data in oil industry, chemical industry, metallurgy and environment [4.31–4.33]. The limitation of experiment to determine the surface tension for the droplet of nanometer size has resulted into the several theoretical models with approximate relations derived from the basic thermodynamics to advanced density functional theory calculations [4.33–4.45]. However, the two major formulations which are the basis for almost all models are developed by Gibbs in 19th century and according to Gibbs, liquid–vapour interfacial energy (γ_{LV}), which measures reversible work to form a new liquid surface per unit area depends on the pressure, temperature and composition of two coexisting bulk phases. The liquid–vapour interfacial energy for interface with curvature depends on the diameter of the

droplet [4.46]. Later with the statistical mechanical consideration, Guggenheim suggested a modification for this size dependent liquid–vapour interfacial energy in the case of small droplets. Subsequently, Tolman in 1949 proposed that the surface tension depends on size of the droplet when its radius does not coincide with equimolar radius. Tolman introduced a parameter called Tolman length which was considered constant and hence the Tolman's formulation failed in predicting the surface tension for droplets with size less than 50 nm. Therefore, the Tolman length has received considerable theoretical attention. However, some issues still remain unresolved such as its temperature, size, potential and sign dependency [4.42, 4.47–4.52].

The nano structured SnO_2 is widely used in areas like photovoltaic energy conversion, preparation of indium tin dioxide transparent conductive thin film coatings, photocatalysis and gas sensors. In order to achieve better gas sensors based on nano structured SnO_2, it is important to have knowledge of relative stability of stoichiometric oxide surfaces. Furthermore, understanding the physical and chemical nature behind the new properties is desired for fabricating the materials for practical applications. The importance of surface is quite vital as it plays key role in many properties of a material particularly when the material is reduced to nano scale. The stability of surfaces which has direct implications for the sensor applications of the oxides is an another area which needs an attention. The (110) facet is found to be the most stable surface in oxides with rutile structure such as TiO_2 and SnO_2 [4.53, 4.54].

We report the calculated surface energy for different facets of anatase TiO_2, rutile TiO_2 and SnO_2 nanoparticles. We have also calculated the size dependent Tolman length of TiO_2 and SnO_2 nanoparticles in order to shed some light on the discrepancy in the sign of

Tolman length. It is important to note that the calculation of surface energy of any material is not possible using classical methods and hence many researchers have used mechanics, thermodynamics, quasi-thermodynamic and statistical mechanics for calculating surface energy of a material. In this work, we use the methodology to calculate the size dependent surface energy and Tolman length of TiO_2 and SnO_2 nanoparticles using the size dependent surface energy without any adjustable parameter under the framework of basic thermodynamics [4.49, 4.54–4.56].

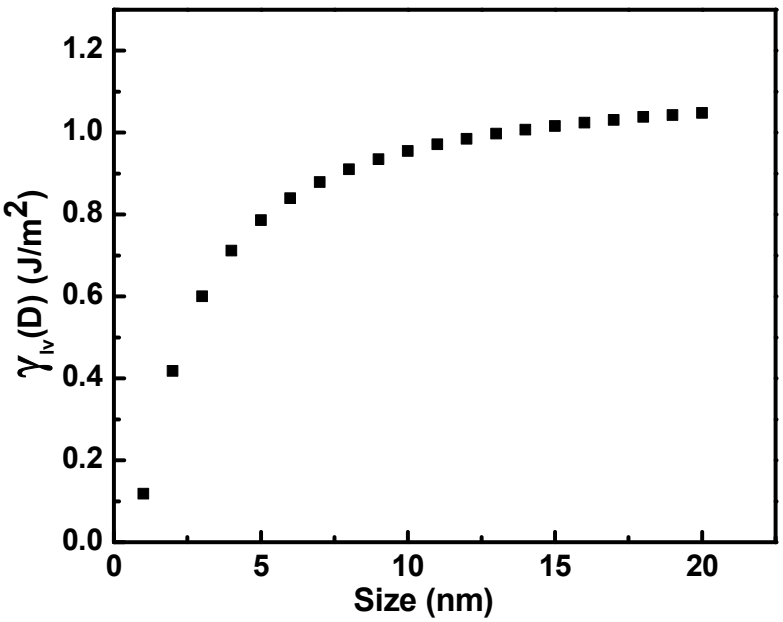

Fig. 4.6 (a)

Fig. presents $\gamma_{LV}(D)$ as functions of size for anatase TiO_2. The related parameters are h=0.3768nm [4.58], $\gamma_{LV}(\infty)=1.05 J/m^2$ [4.57] and $S_b=13R$ for anatase = $108.03 Jmol^{-1} K^{-1}$ [4.57]

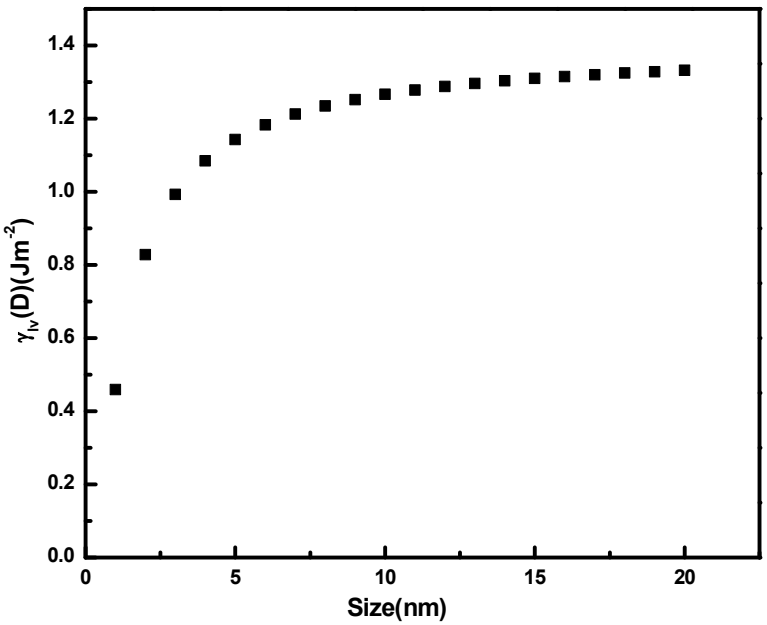

Fig. 4.6 (b)

Above Fig. shows $\gamma_{LV}(D)$ as a function of size for SnO_2 (110) face. The related parameters are h=0.2057nm [4.17], $\gamma_{LV}(\infty)=1.40 J/m^{-2}$ for (110) [4.56] and $S_b=13R=108.03$ $Jmol^{-1}$ K^{-1} [4.57] Fig. 4.6 (a) and (b) shows the calculated size variation of surface tension for anatase TiO_2 and (110) facet of SnO_2 nanoparticles. Fig.4.6 reveals that the surface energy of TiO_2 and SnO_2 nanoparticle decreases with decreasing particle size. This can be understood with a simple fact that as size of the nanoparticle decreases, surface to volume ratio increases, as a result there will be more number of loosely bound surface atoms/molecules making dangling bonds which are responsible for decreasing the energetic difference between surface and interior and consequently there is a decrease in the surface energy of nanoparticles in comparison to bulk material, it is clear from these figures that for both the compounds the surface energy falls rapidly below 10 nm. However to check the accuracy of the present approach, we have also calculated the normalized surface energy of TiO_2 and SnO_2

nanoparticles with size and is presented in Fig. 4.7(a) and (b) along with the plot of the normalized surface energy versus particle size obtained using other methods. The normalized surface energy is the ratio of surface energy of nanoparticles to the surface energy of the bulk at 0K [4.58].

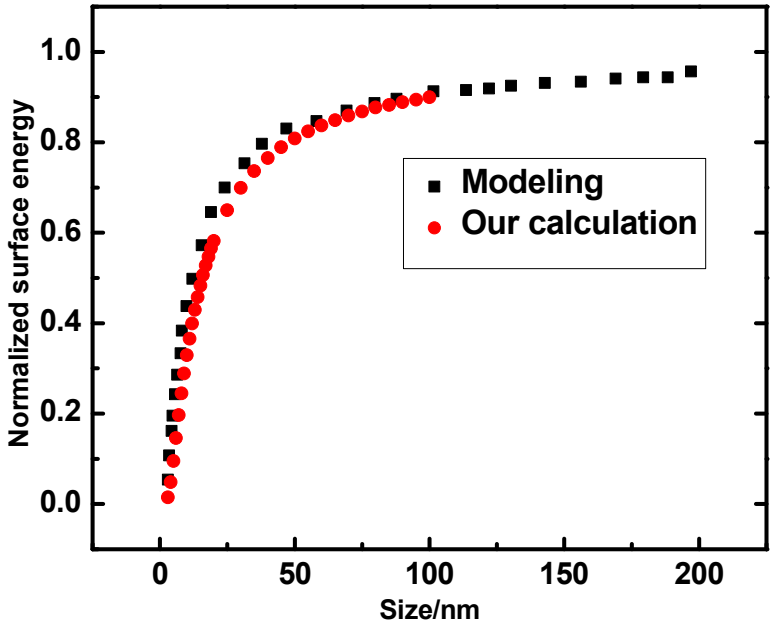

Fig. 4.7 (a)

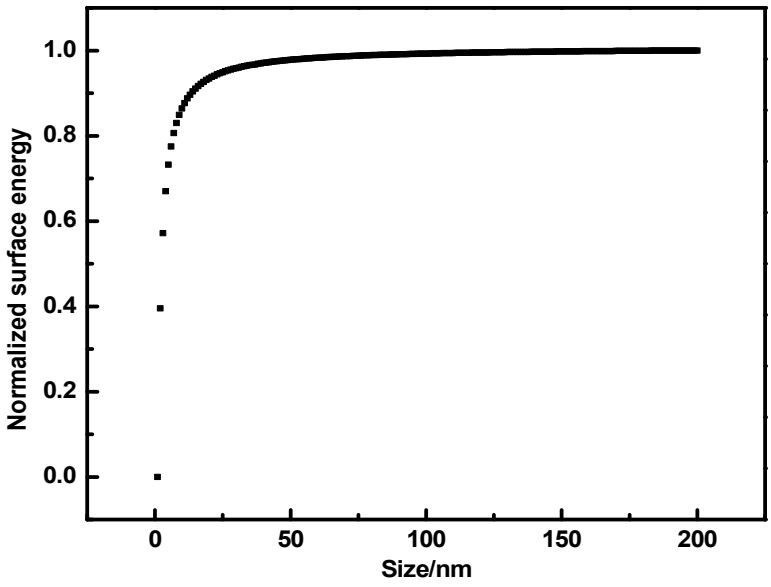

Fig. 4.7 (b)

Fig. presents 4.7(a) $\gamma_{LV}(D)/\gamma_{LV}(\infty)$ as functions of size for rutile TiO_2 and fig. 4.7 (b) presents $\gamma_{LV}(D)/\gamma_{LV}(\infty)$ as a function of size for SnO_2**.** We have used same parameters as described in Fig. 4.6 (a) and (b). Fig. 4.7 reveals a reasonably good agreement between both set of data. The aim of plotting normalized surface energy with size is twofold. First, it reduces the redundant data and helps in knowing more explicitly relative behaviour of surface energy. Secondly and more importantly, to compare our data with other available data which are in normalized form [4.42]. It is known that the surface energy ratio between different facets of crystals is an important parameter in determining the crystalline wulff shapes. These figures clearly depict that the surface energy markedly decreases as the particle size approaches the dimension of the thickness of the surface phase which is consistent with reference [4.58].

Fig. 4.8 (a) and (b) presents the surface energy of different facets of anatase TiO_2 as well as surface tension of (110) rutile facet and variation of surface energy with size for different facets of nano structured SnO_2, respectively.

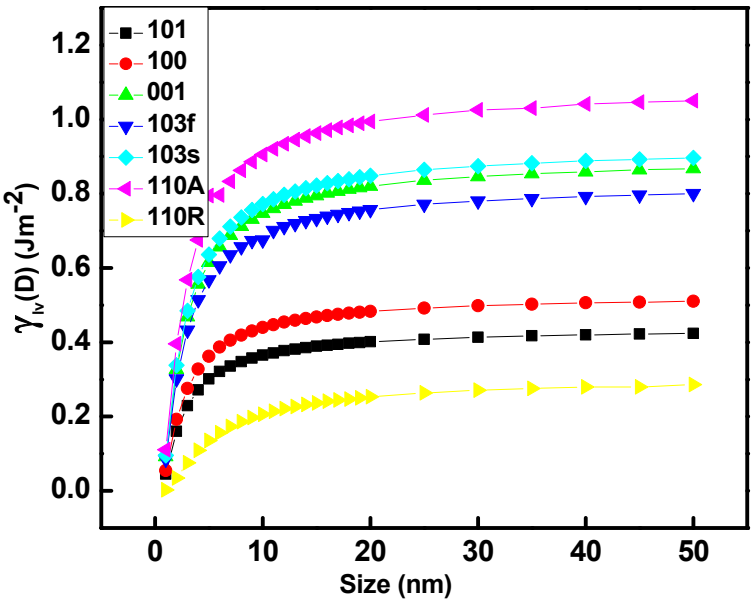

Fig. 4.8 (a)

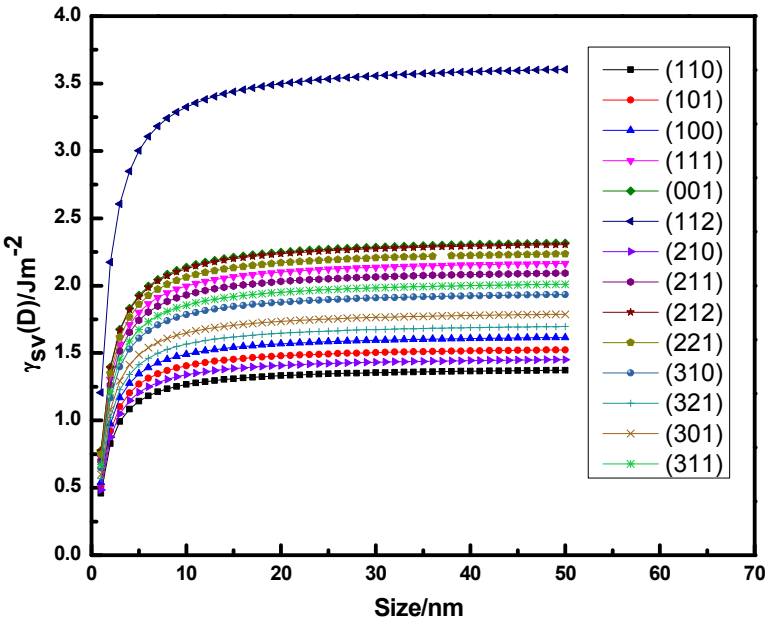

Fig. 4.8 (b)

The value of parameters for bulk system are taken from refs. [4.56, 4.58]. It is seen from these figures that the surface energy for all facets of TiO_2 and SnO_2 nanoparticle decreases drastically with size, particularly below the size of 5nm. However, the surface energy gets saturated above 20 nm for all facets. It is important to note that the results in Fig. 4.8 (a) agree reasonably well with the results obtained from state-of-the-art DFT calculation [4.59]. We also observe that the surface energy for (101) anatase facets of TiO_2 is lowest in comparison to all other facets of anatase TiO_2, which is in good agreement with prediction of Dulub et al. [4.60]. Fig. 4.8(a) shows that the surface energy is highest for the (110) facet of anatase TiO_2 nanoparticles for all sizes. The (101) facet has the lowest surface energy of the considered six facets of anatase TiO_2 and hence is the most stable facet of anataseTiO_2. But (110) facet of rutile TiO_2 shows lower energy than (101) facet of anatase TiO_2. It suggests that rutile structure of TiO_2 is more stable as compared to anatase TiO_2 which is also in

agreement with available literature [4.61]. The second highest surface energy is for the (100) facet, indicating more stability of (100) and (101) facets than (110) facet in the case of anatase structure is in agreement with the experiment [4.62]. In addition, it can also be concluded that the (110) facet contributes largest area to the crystal as this surface has highest surface energy [4.63]. Now turning our attention to the considered (110) facet of rutile TiO_2, we observe that the surface energy is minimum indicating higher stability for (110) facet of rutile. In addition, the temperature also plays an important role in deciding the stable phase. Fig. 4.8(b) presents variation of surface energy with size ranging from 1 nm to 30 nm for different faces of nano structured SnO_2. It can be observed from the figure that the surface energy for (112) and (110) facets have maximum and minimum value of surface energy respectively for given size range. It is an established fact of the thermodynamic theory of Tolman that there is a relation between the size dependency of the surface tension and Tolman length [4.42]. We have also calculated the Tolman length δ(D) for TiO_2 and SnO_2 nanoparticles and presented them in Fig. 4.9 (a) and (b).

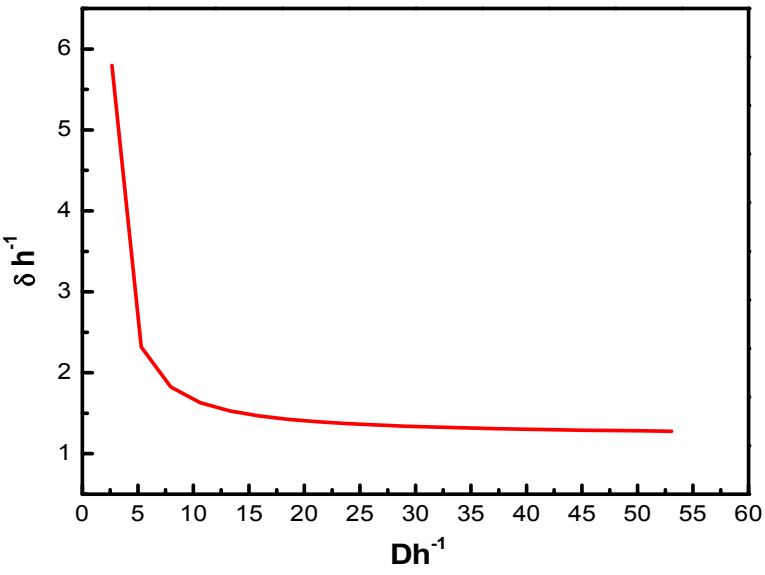

Fig. 4.9 (a)

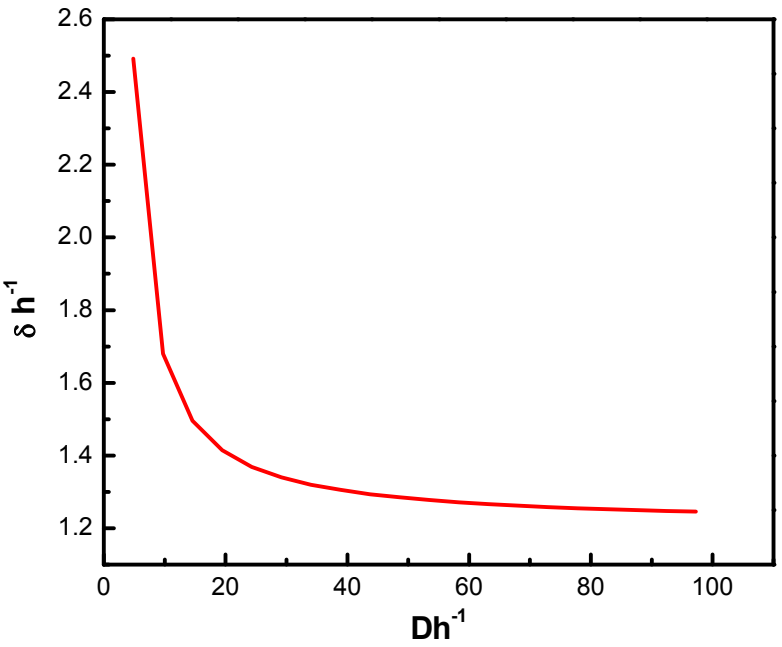

Fig. 4.9 (b)

It can be observed from these figures that the Tolman length of TiO_2 and SnO_2 nanoparticles follows the opposite trend than observed in the case of surface energy. The Tolman length of TiO_2 and SnO_2 nanoparticles decreases as size of the particle increases. The decrease of Tolman length with increasing size indicates that the Tolman length is positive [4.2].

4.4 Catalytic activation energy in SnO_2, TiO_2 and CeO_2 nanoparticles

In recent years, enormous efforts have been devoted to study the size and shape dependence of nanoparticles to understand the catalytic and electro catalytic performances [4.64-4.66]. Nanoparticles of different materials act as efficient catalysts for oxidation of hydrocarbons, C-C coupling, hydrogenation, dehydrogenation, redox and other chemical transformations [4.65, 4.67-4.78]. Past studies show that the TiO_2 is a promising candidate for the decomposition of wide variety of organic and inorganic moieties in both liquid and gas phases [4.79-4.82]. The nano scale cerium dioxide (CeO_2) has also advantages as a

support for catalysis since it can enhance the reactivity for the oxidation reaction and CO oxidation when supported to gold nanoparticles [4.83, 4.84]. Although nanoparticles of tin dioxide (SnO_2) are of less interest particularly for catalytic applications, Sharghi et al., [4.85] have found that the SnO_2 nanoparticles are highly reactive in the Knoevenagel condensation process. In this section, we present results of calculated size and shape dependent catalytic activation energy (E_C) of three different nanostructures i.e., titanium dioxide (TiO_2), cerium dioxide (CeO_2) and tin dioxide (SnO_2).

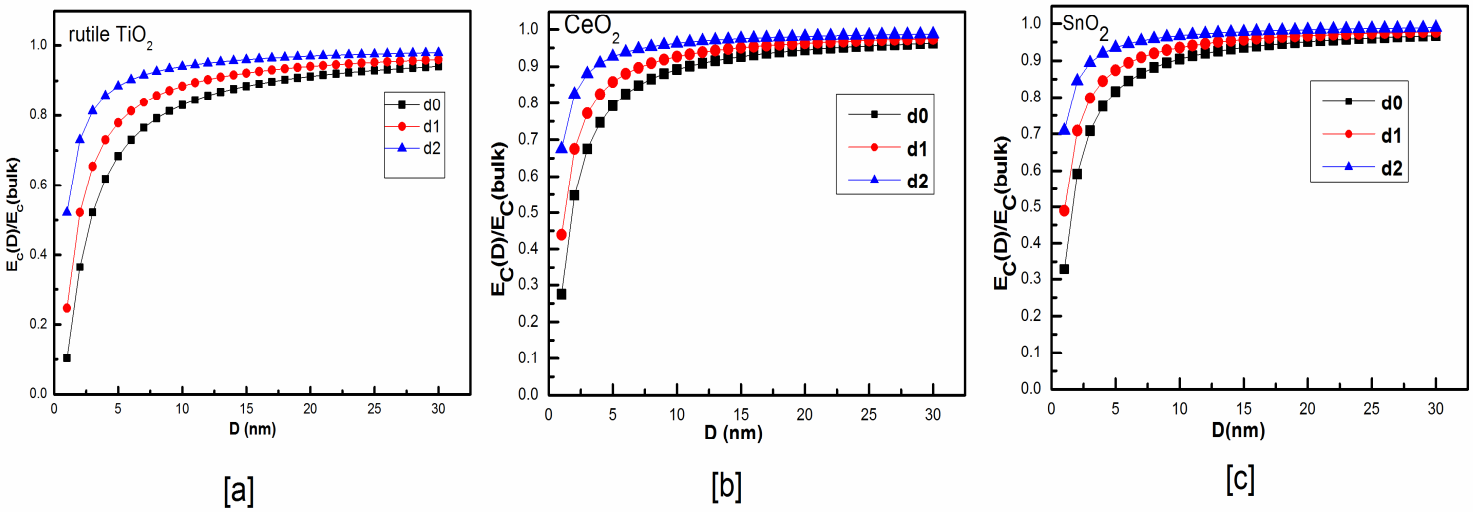

Fig. 4.10

Above Fig. presents $E_C(D)/E_C(\infty)$ as a function of size and dimensions for nano structured (a) rutile TiO_2 (b) CeO_2 and (c) SnO_2**.** Fig. 4.10 (a) presents the variation of $E_C(D)/E_C(\infty)$ (ratio of size dependent activation energy to its bulk counterpart) of rutile TiO_2 nanoparticles of different dimensions which shows that the catalytic activation energy decreases as the size of the TiO_2 nanoparticle decreases. The value of activation energy rapidly decreases below 5 nm. It is clear from this figure that after 15 nm, the ratio of catalytic energies becomes almost

constant. The figure also depicts that the catalytic activation energy is minimum for spherical nanoparticles while it is maximum for the two dimensional case. This indicates that the spherical nanoparticles can act as better catalysts compared to one and two dimensional nanostructures. The decrease in the catalytic activation energy with the decreasing size reveals efficiency of nanoparticles to catalyze any chemical reaction. Figs. 4.10 (b) and (c) presents the size and dimension dependence of $E_C(D)/E_C(\infty)$ for another nanoparticles of this group CeO_2 and SnO_2 respectively. Both figures show similar behaviour as observed in the case of TiO_2 nanoparticles. However, it saturates after 10 nm in the case of CeO_2 and SnO_2 nanostructures in contrast to TiO2 nanostructure. Spherical nanoparticles indicate good catalytic performance rather than nano wires and thin films.

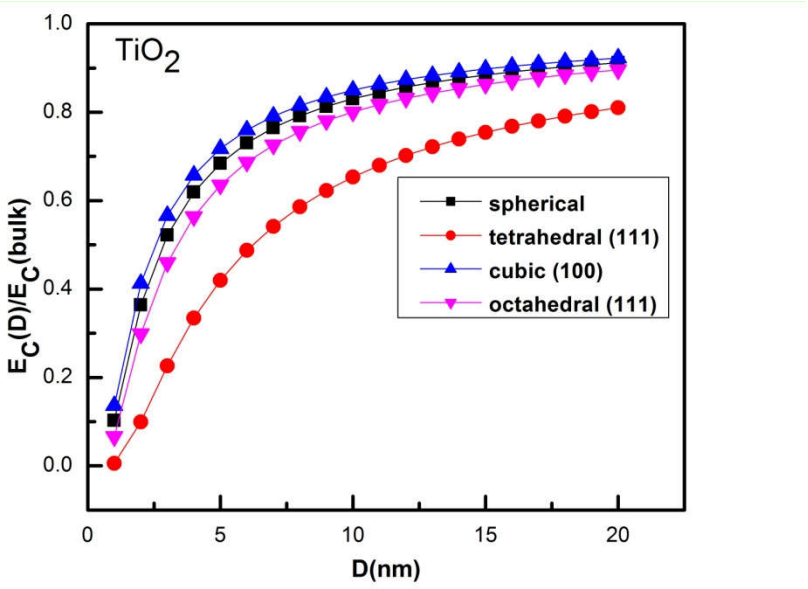

Fig. 4.11

Fig. 4.11 shows the variation of $E_C(D)/E_C(\infty)$ with size and different shapes of TiO_2 nanoparticles. For a particular size, a tetrahedral shaped particle with (111) facet exhibits minimum value of E_C compared to octahedral and cubic shaped nanoparticles. It can be

observed from the figure that the cubic nanoparticles are having the maximum value of E_C for a given size. This nature of catalytic activation energy indicates that the tetrahedral shaped nanoparticles are the most catalytically active. For CeO_2 and SnO_2 nanoparticles, we obtain similar behaviour where tetrahedral shape of the particles show higher value of E_C. It can be explained by a fact that the small tetrahedral particles have sharp edges and corners. It is found that the atoms located on these sites are chemically very active. In cubic nanoparticles, most of the atoms are located on (100) facets and found to be least active, consequently these particles possess higher value of E_C [4.64].

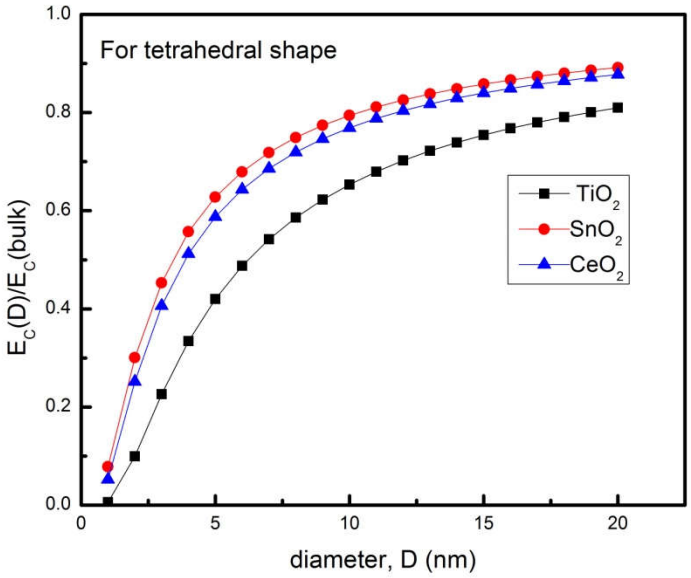

Fig. 4.12

$E_C(D)/E_C(\infty)$ as a function of size for tetrahedral shaped TiO_2, CeO_2 and SnO_2 nanoparticles is presented in fig. 4.12. It shows comparison of all the three tetrahedral shaped nanostructures (i.e., TiO_2, CeO_2 and SnO_2) in terms of size dependent catalytic activation energy. It is clear from the figure that the TiO_2 nanoparticles have minimum catalytic activation energy which implies that the nano structured TiO_2 can be considered as an

efficient candidate for catalytic activities. Although nano sized SnO_2 has advantage for a particular reaction when used as a catalyst, it shows the least chemical activity in present study while CeO_2 has the intermediate value of E_C between TiO_2 and SnO_2. The similar trend of size and shape dependent catalytic activation energy is reported in case of platinum nanoparticles

References

4.1 P.A. Bhatt, A. Pratap, P.K. Jha, J. Therm. Anal. Calorim. 110, 535 (2012).

4.2 P.A. Bhatt, S. Mishra, P.K. Jha, A. Pratap, Physica B. **461,** 101 (2015).

4.3 M. Gratzel, Nature. **414,** 338 (2001).

4.4 X. Chen, S.Mao, Chem.Rev. **107,** 2891 (2007).

4.5 N.G. Deshpande,Y.G. Gudage,R. Sharma,J.C. Vyas,J.B. Kim,Y.P. Lee, Sens. Act. B: Chem. **138,** 76 (2009).

4.6 V. Krivetskiy, A.Ponzoni, E.Comini, S.Badalyan, M.Rumyantseva, A.Gaskov, Electroanalysis. **22,** 2809 (2010).

4.7 H.J. Snaith,C.Ducati, Nano Lett.**10,** 1259 (2010).

4.8 C. Manifacier,Thin Solid Films. **90,** 297 (1982).

4.9 Y.Hao,W.Wu, L.L.Xie, 2nd International Conference on Chemical,Biological and Environmental Engineering (ICBEE),Cairo,p.96 (2010).

4.10 Q.Q. Wang, B.Z.Lin, B.H.Xu, X.L.Li, Z.J.Chen, X.T.Pian, Microporous Meso-porous Mater.**130,** 344 (2010).

4.11 L.H. Zhang, P.J. Li, Z.Q. Gong, X.M. Li, J. Hazard. Mater. **158,** 478 (2008).

4.12 A.K.Singh, U.T.Nakate, Adv.Nanopart.**2,** 66 (2013).

4.13 M.J. Takagi, J. Phys. Soc. Japan. **9,** 359 (1954).

4.14 S. K. Gupta, M. Talati, P. K. Jha, Mater. Sci. Forum. **570,** 132 (2008).

4.15 W. H. Qi, Physica B. **368,** 46 (2005).

4.16 W. H. Qi, M. P. Wang, Mat Chem & Phys. **88,** 280 (2004).

4.17 C.C. Yang , S. Li, J. Phys. Chem. B. **112,** 14193 (2008).

4.18 S. Cava, T. Sequinel , S.M. Tebcherani , M.D. Michel, S.R. Lazaro, S.A. Pianaro. J. Alloys. Compd. **484,** 877 (2009).

4.19 V.V. Hoang, J. Phys. D. **40,** 7454 (2007).

4.20 M. Gupta, A. Gupta, R. Gupta and T. Gutberlet, J. of phase equilibria and diffusion **26,** 458 (2005).

4.21 B. Kamp, R. Merkle, J. Maier, Sens. Acuat. B. **77,** 534 (2001).

4.22 Q. Jiang, S.H. Zhang, J.C. Li, Solid State Communications **130,** 581(2004).

4.23 Table of Periodic Properties of the Elements, Sargent-Welch Scientific company, Skokie, IL, 1980.

4.24 R. Narayana, M.A. El-Sayed, Nano Lett. **4,** 1343 (2004).

4.25 G. Li, B. Goater , B.F. Woodfield ,L. Li, Appl. Phys. Lett. **85,** 2059 (2004).

4.26 D.J. Cooke, S.C. Parker , D.J. Osgutherpe, Phys. Rev. B. **67,** 134306 (2003).

4.27 P. A. Bhatt, A. Pratap, P. K. Jha, AIP Conf. Proc. **1536,** 237 (2013).

4.28 Q. Jiang, H. M. Lu, Surf. Sci. Rep. **63,** 427 (2008).

4.29 F. Bechstedt, Principles of Surface Physics, 4thed, Springer, NewYork, (2003).

4.30 K.K. Nanda, Phys. Lett. A. **376,** 1647 (2012).

4.31 E.K. Goharshadi, M.Abbaspour, Chem.Phys. **328,** 379 (2006).

4.32 X. Yong-Qiang, Y.Xin-Cheng, C.Zi-Xiang, L.Wei-Peng, J. Phys. Chem. B, **115,** 109 (2011).

4.33 I. Hadjiagapiou, J. Phys.:Condens. Matter **6,** 5303 (1994).

4.34 V.M. Samsonov, L.M.Shcherbakov, A.R.Novoselov, A.V.Lebedev, Colloids Surf. A, **160,** 117 (1999).

4.35 V.M. Samsonov, N.Yu.Sdobnyakov, A.N.Bazulev, Surf. Sci. **532–535,** 526 (2003).

4.36 S. Heidenreich, H.Buttner, J. Aerosol Sci. **26,** 335 (1995).

4.37 V.M. Samsonov, N.Y. Sdobnyakov, A.N. Bazulev, Colloids Surf. A. **239,** 113 (2004).

4.38 M. Matsumoto, K. Tanaka, Fluid. Dyn. Res. **40,** 546 (2008).

4.39 D. Mukherjee, A. Prakash, M. R. Zachariah, J. Aerosol Sci. **37,** 1388 (2006).

4.40 L.N. Protasova, E. V. Rebrov, Z. R. Ismagilov, J. C. Schouten, Microporous Mesoporous Mater.**123,** 243 (2009).

4.41 A. Troster, K. Binder, Phys. Rev. Lett. **107,** 265701 (2011).

4.42 R.C. Tolman, J. Chem. Phys. **17,** 333 (1949).

4.43 C. Bre'chignacv, H. Busch, Ph. Cahuzac, J. Leygnier, J.Chem.Phys. **101,** 6992 (1994).

4.44 U. Naher, S. Bjornholm, S. Frauendorf, F. Garcias, C.Guet, Phys. Rep. **285,** 245 (1997).

4.45 D. Xie, M. P. Wang, W. H. Qi, J. Phys.:Condens. Matter **16,** L401 (2004).

4.46 J.W. Gibbs, The Collected Works of J. Willard Gibbs, Longmans, Green and Company,NewYork,1928.

4.47 E. A. Guggenheim, Trans. Faraday Soc. **35,** 397 (1940).

4.48 R.C. Tolman, J. Chem. Phys.**17,** 118 (1949).

4.49 H.M. Lu, Q. Jiang, Langmuir **21,** 779 (2005).

4.50 J.C. Rowlinson, B. Widom, Molecular Theory of Capillarity, Clarendon Press, Oxford, (1982).

4.51 V.B. Fenelonov, G. G. Kodenyov, V. G. Kostrovsky, J. Phys. Chem. B. **105,** 1050 (2001).

4.52 V. Talanquer, D. W. Oxtoby, J. Phys. Chem. **99,** 2865 (1995).

4.53 P. A. Mulheran, J. H. Harding, Model. Simul. Mater. Sci. Eng. **1,** 39 (1992).

4.54 J. Oviedo, M. J. Gillan, Surf. Sci. **463,** 93 (2000).

4.55 D. Kashchiev, J. Chem. Phys.**118,** 9081 (2003).

4.56 B. Slater, C. Richard, A. Catlow, D. H. Gay, D. E. Williams,V. Dusastre, J. Phys. Chem. B. **103,** 10644 (1999).

4.57 C. C. Yang, Q. Jiang, Mater. Sci. Eng. B **131,** 191 (2006).

4.58 H. Zhang, J. F. Banfield, J. Mater. Res. **15,** 437 (2000).

4.59 M. Lazzeri, A. Vittadini, A. Selloni, Phys. Rev. B. **63,** 155409 (2001).

4.60 O. Dulub, U. Diebold, J. Phys.: Condens. Matter **22,** 084014 (2010).

4.61 D. A. H. Hanaor, C.C. Sorrell, J. Mater. Sci. **46,** 855 (2011).

4.62 Y. W. Chung, W. J. Lo, G. A. Somorjai, Surf. Sci. **64,** 588 (1977).

4.63 M. Ramamoorthy, D. Vanderbilt, R. D. King-Smith, Phys. Rev. B. **49,** 16721 (1994).

4.64 R. Narayanan and M.A. El-Sayed, Nano Lett. **4,** 1343 (2004).

4.65 C. Burda, X.B. Chen, R. Narayanan and M.A. El- Sayed, Chem. Rev. **105,** 1025 (2005).

4.66 Y. Li, J. Petroski and M.A. El-Sayed, The J.of Phy. Chem. B. **104,** 10956 (2000).

4.67 X. Zhou, W. Xu, G. Liu, D. Panda, P. Chen, J.of the Ame. Chem. Soc. **132,** 138 (2010).

4.68 G. A. Somorjai, A. M. Contreras, M. Montano, R. M. Rioux, Proc. of The Nat. Aca. of Sci. of the United States of Ame. **103,** 10577 (2006).

4.69 G. Ertl, H. Knozinger, J. Weitkamp, (ed.) Handbook of heterogeneous catalysis, Weinheim: Wiley-VCH (1997).

4.70 A. T. Bell, Science, **299,** 1688 (2003).

4.71 M. Chen, D. W. Goodman, Acc. of chem. res. **39,** 739 (2006).

4.72 R. M. Crooks, M. Zhao, L. Sun, V. Chechik, L. K. Yeung, Acc. of chem. res., **34,** 181 (2001).

4.73 Lewis, L.N. Chem. Rev. **93,** 2693 (1993).

4.74 D. Astruc, F. Lu, J. R. Aranzaes, Angew. Chem. Int. Ed. **44,** 7852 (2005).

4.75 A. Roucoux, J. Schulz, H. Patin, Chem. ReV. **102,** 3757 (2002).

4.76 G. Schmid, Editor, Nanoparticles from Theory to Application, Wiley- VCH Verlag GmbH & Co. KGaA: Weinheim (2004).

4.77 W. Wasylenko, H. Frei, Phys. Chem. Chem. Phys. **9,** 5497 (2007).

4.78 M.C. Kung, R.J. Davis, H.H. Kung, J. Phys. Chem. C. **111,** 11767 (2007).

4.79 V. Mankad, S. K. Gupta, P.K. Jha, Physica E. **44,** 614 (2011).

4.80 S.K. Gupta, R. Desai, P.K. Jha, S. Sahoo and D. Kirin, J. Raman Spectrosc. **41,** 350 (2010).

4.81 P.K. Jha, Editor, Titanium Dioxide: Applications, Synthesis and Toxicity, Nova Science Publications, New York (2013).

4.82 R. Desai, S.K. Gupta, S. Mishra, P. K. Jha and A. Pratap, Int. J. Nanoscience. **10,** 1249 (2011).

4.83 M.N. Guo, C.X. Guo, L.Y. Jin, Y.J. Wang, J.Q. Li, M.F. Luo, Mater. Lett. **64,** 1638 (2010).

4.84 S. Carrettin , P. Concepción , A. Corma , J. M. L. Nieto, V.F. Puntes , Angew. Chem. Int. Ed. **43,** 2538 (2004).

4.85 H. Sharghi, S. Ebrahimpourmoghaddam, R. Memarzadeh, S. Javadpour, J. Iran. Chem. Soc. **10,** 141 (2013).

4.86 H. M. Lu, X. K. Meng, The J. of Phy. Chem. C. **114,** 1534 (2010).